Filter Bank Multi-Sub-Band Transmission for Optical Systems with Mode Multiplexing

Lailson F. dos Santos*, **Filipe M. Ferreira**†, **Andrew D. Ellis**†, **Darli A. A. Mello***

**School of Electrical and Computer Engineering, University of Campinas (UNICAMP), Campinas, Brazil*
†*Aston Institute of Photonic Techonogies, Aston University, Birminghan, B4 7ET, UK*

DOI: XX.XXX/JPHOT.2018.XXXXXXX

This is an extended version of [1]. Corresponding author: Lailson F. dos Santos (lailson@decom.fee.unicamp.br).

Abstract: Mode-multiplexed optical transmission is subject to mode coupling and potentially large differential mode delays. In most recent implementations, these effects are compensated for at the receiver by complex adaptive multiple-input multiple-output (MIMO) equalizers. Although frequency-domain MIMO equalization requires a moderate complexity compared to time-domain equalization, the long required fast Fourier transforms (FFTs) may face implementation issues. In this paper, we evaluate an alternative transceiver architecture based on sub-band partitioning, implemented by filter banks, which enables concurrent time-domain equalization. Single-carrier (SC) and multi-sub-band (MSB) mode division multiplexing (MDM) transmission are simulated using frequency-domain equalization (FDE) and time-domain equalization (TDE), respectively. Their performance is compared in terms of static transmission performance, channel tracking capability, phase noise tolerance, and computational complexity. The results indicate that compared with an equivalent SC solution, the MSB architecture provides a high degree of parallelism at the cost of a penalty of 0.7-to-1.3 dB for a laser linewidth of 25-to-100 kHz and a moderate increase in complexity.

Index Terms: Sub-band transmission, space-division multiplexing, MIMO equalization, mode multiplexing.

1. Introduction

The sustained growth of Internet traffic raises concerns about the scalability of current core optical networks, and motivates the study of disruptive technologies such as space-division multiplexing (SDM). SDM can be implemented in a number of ways, including multicore fibers (MCFs) and multimode fibers (MMFs). Signals conveyed by MCFs with uncoupled cores are easy to couple and switch, but demand careful crosstalk (XT) management across all the network elements. On the other hand, MMFs require typically multiple-input multiple-output (MIMO) processing to separate the signals multiplexed over the multiple orthogonal modes [2], [3], [4]. In this case, equalization and source separation complexity scales with the accumulated differential mode delay (DMD), which depends on the linear mode coupling strength. In the weak coupling regime DMD grows linearly with the fiber length [5], [6]. In the strong coupling regime the mode-group delays (MGDs) are averaged by the mode mixing, such that DMD grows with the square root of the fiber length [5].

MMFs operating in a strong coupling regime are an interesting alternative to reduce the length of the optical channel, and consequently the complexity of MIMO equalizers [7]. But this complexity still remains a challenge for mode-multiplexing systems with high DMD and low or moderate levels of mode coupling [2], [3]. Although in frequency-domain equalization (FDE) the computational complexity scales with the logarithm of the delay spread [8], [9], the application-specific integrated

circuit (ASIC) area reserved for the fast Fourier transforms (FFTs) and their inverse (IFFTs) may become excessively large, and long dynamic channel equalizers may face implementation issues [10].

A promising alternative to avoid large FFT sizes and improve the degree of parallelism of the receiver DSP is to split the spectrum into smaller sub-bands and carry out source separation and deconvolution in parallel for the individual subchannels [11]. One possible solution is the use of orthogonal frequency division multiplexing (OFDM), however, its application in systems with mode multiplexing is complicated by the need for long cyclic prefixes due to large delay spreads. This drawback has been circumvented by sub-band partitioning using Nyquist-shaped carriers, as reported in [12], [13] to mitigate DMD in MCF fibers with multi-mode cores. In both works the generated sub-bands were frequency-multiplexed and demultiplexed independently. Alternatively, low-complexity sub-band solutions based on polyphase filter banks have been widely investigated in the context of wireless communications systems [14]. This idea has been also validated in conventional polarization multiplexed optical systems using twice-underdecimated filter banks [15]. This sub-band structure has been applied to mitigate chromatic dispersion (CD) [11], [16], [17], [18] and non-linear effects [19], [20], [21], [22]. Polyphase filter bank architectures have also been employed in the context of MIMO equalization for MMFs in [10], where the twice-underdecimated filter bank architecture was adapted to achieve fast convergence in an OFDM system with weakly coupled spatial channels.

We investigated in [1] the performance of the multi-sub-band (MSB) architecture using polyphase filter banks in MIMO SDM equalization with digitally-generated subchannels for a static channel. The performance of a single-carrier (SC) system with time-domain equalization (TDE) was compared with that of an MSB-TDE architecture at the same data rate and bandwidth, using Monte-Carlo simulations. In systems with a large delay spread, FDE is preferable compared to TDE in terms of complexity. However, in sub-band systems, in which the channel length is reduced according to the number of sub-bands, the channel becomes shorter, and TDE is still an interesting choice. Therefore, in this paper we extend the results of [1], comparing the MSB-TDE architecture with that of an SC-FDE solution. We also evaluate both systems under dynamic channel conditions, and assess their resilience to laser phase noise. Finally, we compare their complexity in terms of the number of complex multiplications. The remainder of this paper is organized as follows. Section 2 details the investigated MSB system. Section 3 describes the simulation setup and results. Section 4 compares the complexity of the SC-FDE and MSB-TDE transceivers. Section 5 concludes the paper.

2. Multi Sub-Band Architecture for Mode Multiplexing

2.1. Transmitter

Figure 1 shows the transmitter diagram of the MSB system investigated in this paper. This basic structure is replicated for each of the N_m spatial modes. Data generated by a binary source is first mapped into a complex signal constellation at a rate R_{sc}, which is equivalent to that of a SC system. These symbols are divided into N_{sb} sub-bands at a rate R_{sc}/N_{sb}. Then, the data is sent to a polyphase synthesis bank implemented with $N_{sb}+1$ sub-bands. A guard sub-band containing zeros is included in position $(N_{sb}+1)/2+1$ to avoid edge effects [17], such as distortions caused by a non-ideal digital-to-analog converter (DAC). Although the symbol time $T_{sb} = (N_{sb}+1)/R_{sc}$ is increased by the insertion of the guard band, the signal bandwidth still corresponds to the single-carrier case, as half of the null sub-band appears at both edges of the spectrum. After parallel to serial conversion, the complex signals are pre-distorted and fed into an in-phase and quadrature Mach-Zehnder modulator (IQ-MZM) for electro-optical conversion [23]. Finally, the signals are multiplexed into the corresponding spatial modes and sent to the optical channel. The synthesis filter bank architecture is depicted in Fig. 2. First, the serial signal is parallelized, so that it can be processed by a discrete Fourier transform (DFT) with $N_{sb}+1$ points. A root-raised cosine (RRC) filter with impulse response $h_{PF}[n]$ is used as prototype. The polyphase filter of the sb^{th} sub-band

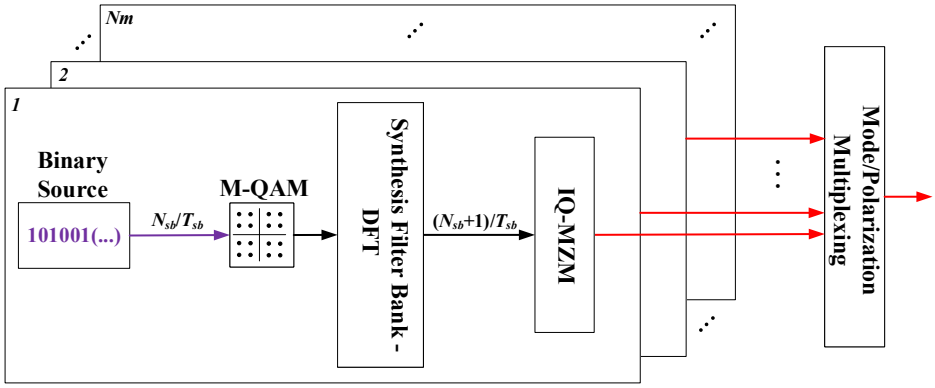

Fig. 1. MSB transmitter architecture.

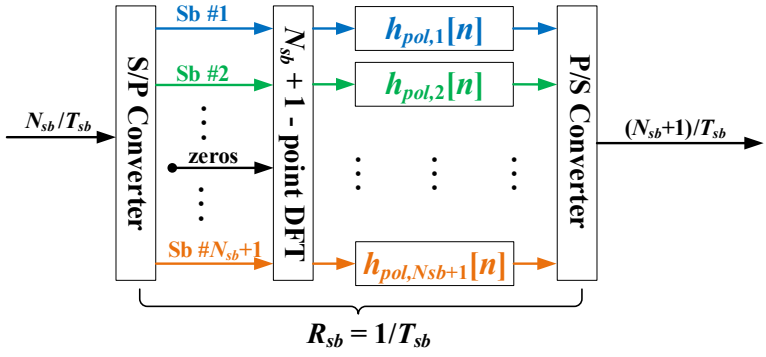

Fig. 2. Synthesis filter bank architecture.

is calculated by means of the polyphase decomposition of $h_{PF}[n]$ [24], [25]:

$$h_{pol,sb}[n] = h_{PF}[(N_{sb}+1)n + (sb-1)], \quad 1 \leqslant sb \leqslant N_{sb}+1 \tag{1}$$

The final electric signal is obtained after parallel-to-serial conversion.

2.2. Receiver

The MSB receiver structure is shown in Fig. 3. After optical mode and polarization demultiplexing, the N_m signals are converted into the electrical domain by receiver front-ends [26], [27] and are sampled at a rate of $(N_{sb}+1)/T_{sb}$. Note that the MSB architecture requires nearly half the sampling rate of the SC receiver, which typically operates with 2 samples per symbol (SpS). Each mode-demultiplexed signal is then subject to chromatic dispersion compensation using a frequency-domain static filter [28]. Then, the signal follows to the twice-underdecimated filter bank (2x Udeci-FB) based on polyphase filters that are matched to the transmitted waveforms [15]. Although the DSP architecture receives a signal with 1 SpS in each sub-band, the 2x-Udeci-FB block produces 2 SpS for subsequent equalization. After that, the signals are sent to N_{sb} (N_mxN_m- MIMO) adaptive equalizers, one for each sub-band. The structure of the MIMO adaptive filters is a generalization of the 2×2-MIMO butterfly equalizer for polarization multiplexed (PM) signals [28], [29]. Finally, the bit error rate (BER) is calculated for all sub-bands of each spatial mode.

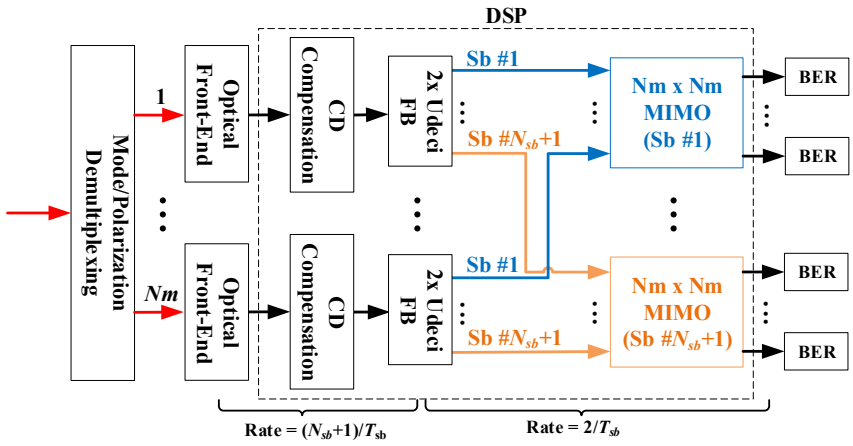

Fig. 3. MSB receiver architecture. The red arrows indicate optical conncections, while the remaining arrows correspond to DSP interconnections.

3. Simulation Setup and Results

3.1. Simulation setup

The simulations for both the MSB and SC systems are based on the 16-QAM modulation format at a bit rate of 256 Gb/s per mode. The SC transmission setup generates Nyquist-shaped pulses (RRC shaping filter with 513 coefficients and 0.01 roll-off factor) at 32 Gbaud. For the MSB system, the RRC prototype filter is implemented with 0.01 roll-off factor and the length of the polyphase filters is set to 128 taps. The MSB system was simulated with a number of sub-bands ranging from 3 to 11, which is in-line with previous publications in the area [17]. As the symbol duration is proportional to the number of sub-bands, an excessively large number of sub-bands can affect the phase recovery performance. An electric receiver bandwidth of 16 GHz is assumed in all setups. Adaptive equalizers implement FDE for the SC system, and TDE for the MSB system. The BER is counted by averaging the results obtained, in each spatial mode, over 50,000 symbols (in the MSB case, the calculation is performed over two runs of 25.000 symbols each).

The optical channel setup consists of noise loading and a 100-km few-mode fiber model containing -30 dB/km crosstalk and 20 ps/km DMD, simulated according to [30], [31]. Here we follow the method described in [30] to solve the differential mode equations describing linear mode coupling in few-mode fibers given waveguide imperfections introduced during the fabrication process or by mechanical stresses imposed in the deployment. According to this method, the core-cladding fluctuations are discretized by dividing the fiber in multiple sections, each with a random displacement of the core center position, allowing semi-analytical solutions of the coupling operator [32]. In this model, the linear mode coupling strength is set using a fixed amount of radial displacement and a random azimuth displacement given by a uniform distribution. In this way, it was shown in [30] that at each step a random amount of crosstalk is introduced among non-degenerate modes that in average approximates the desired level. This method has been proven accurate in the linear power regime, matching the analytical predictions for the group delay statistics in FMF links for different transmission lengths (10 m to 10,000 km), in any coupling regime (-70 dB/100 m to 0 dB/100 m), with and without group delay management. The simulated CD vector at 1550 nm is (22.18, 21.55, 22.15, 22.15, 21.84, 21.84) ps/(km·nm) and the group delay vector is (-1.12, -11.26, -2.53, -2.53, 8.73, 8.73) ps/km for modes (LP01, LP02, LP11a, LP11b, LP21a, LP21b), respectively, according to [33].

3.2. Static channel performance

We first evaluate the SC and MSB architectures with noise loading, to detect potential implementation penalties. For the SC system an initial sequence of 200,000 symbols is used for supervising the convergence of the 12×12 MIMO equalizer (corresponding to 6 linearly polarized (LP) modes and the respective polarization modes), which is updated by the least-mean squares (LMS) algorithm [34]. After the training phase, the filter coefficients remain static, as the simulated channel does not vary over time. For the MSB system a training sequence of 30,000 symbols is used for convergence of the N_{sb} (12×12 MIMO) adaptive equalizers, implemented individually in each sub-band. After training, the filter coefficients remain static.

The bit error rate (BER) versus optical signal to noise ratio (OSNR) performances of both systems are shown in Fig. 4. The dashed lines indicate the case where only one sub-band is simulated at a time, without neighbors. Here, the MSB and SC systems exhibit equivalent performance. However, if all sub-bands are activated, a 0.5-dB penalty is observed for MSB with 3 and 11 sub-bands for BER = 4×10^{-3}. Such penalties due to inter-sub-band interference are a well-known phenomenon in MSB architectures [17], and are also present in our simulation setup.

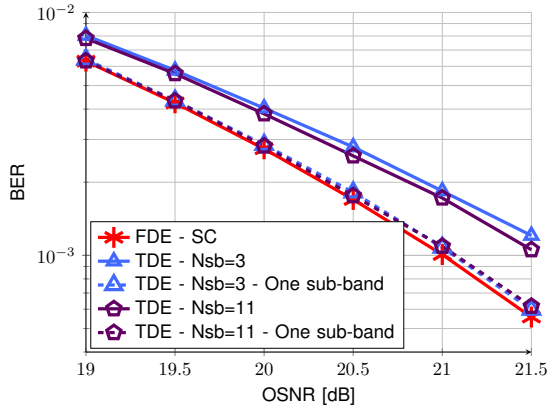

Fig. 4. SC and MSB performances with noise loading; solid line with stars: SC system using FDE; solid lines: MSB system using TDE with 3 (triangles) and 11 (pentagons) sub-bands; dashed lines: MSB system using TDE where one sub-band is simulated at a time for 3 (triangles) and 11 (pentagons) sub-bands, respectively.

Figure 5 shows the OSNR required to achieve a BER of 4×10^{-3} ($OSNR_{req}$), versus the number of equalizer filter taps, for different configurations on a static channel. The performance with noise loading of the SC and MSB systems is presented in Fig. 5(a), as a reference. For sufficiently long dynamic equalizers, the $OSNR_{req}$ stabilizes in 19.5 dB for SC and approximately 20 dB for all simulated MSB configurations, confirming the 0.5-dB penalty for the MSB system due to inter-sub-band interference. The SC performance for configurations with crosstalk, DMD and uncompensated CD are shown in Fig. 5(b). The DMD alone increases the required filter length from 20 taps to approximately 250 taps, achieving the same $OSNR_{req}$ of 19.5 dB. When CD is left uncompensated, the minimum filter length raises to 280 taps. The MSB system subject to crosstalk and DMD is shown in Fig. 5(c). The filter length required for a satisfactory performance varies from 30 taps (11 sub-bands) to 70 taps (3 sub-bands). The results of the case where CD is left uncompensated are shown in Fig. 5(d), and indicate that the impact of CD on the equalizer filter length is negligible. Indeed, the delay spread of the residual CD is expected to increase the length of the adaptive equalizers. Although this effect is observed in the SC system (with an increase in filter length by 30 taps), it is negligible in the MSB system for the simulated configuration. This can be explained by the fact that the delay spread due to the CD decreases quadratically with the transmission bandwidth and, consequently, with the number of sub-bands, as pointed out in [17]. Thus, although SC systems require an increase in complexity due to CD, this increase is

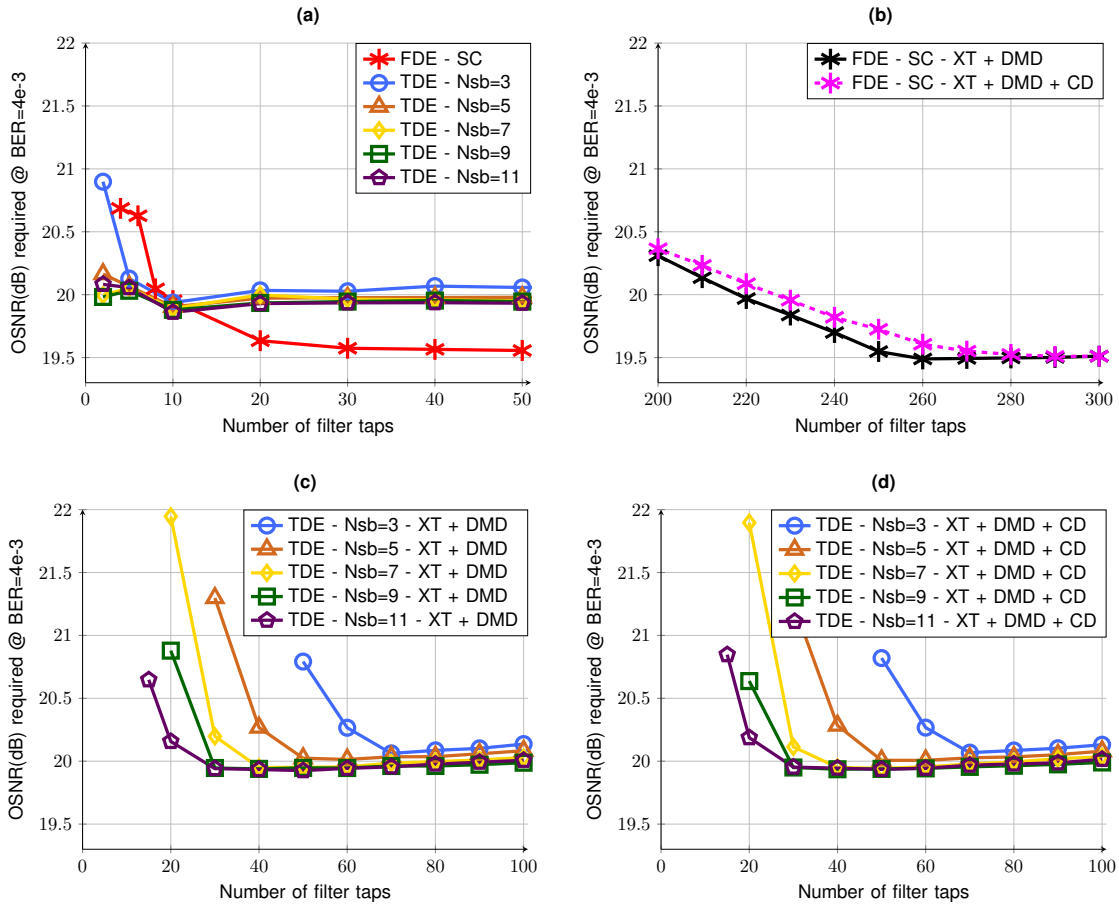

Fig. 5. (a) MSB and SC transmission with noise loading. (b) SC transmission with -30 dB/km crosstalk, 20 ps/km DMD, and both fully compensated (solid line) and uncompensated (dashed line) CD. (c) MSB transmission with -30 dB/km crosstalk, 20 ps/km DMD, and fully compensated CD. (d) MSB transmission with -30 dB/km crosstalk, 20 ps/km DMD, and uncompensated CD. Stars: SC system using FDE. Remaining symbols: MSB system for 3 (circles), 5 (triangles), 7 (diamonds), 9 (squares) and 11 (pentagons) sub-bands using TDE.

strongly reduced with the implementation of MSB systems, due to its intrinsic architecture.

Figure 6 shows the convergence time of SC and MSB systems with crosstalk and DMD for a static channel. The length of the equalizer was selected according to Figs. 5(b) and 5(c), and step sizes were optimized for every condition. The SC case requires approximately 120,000 symbols to converge (see Fig. 6(a)), which is significantly higher than in usual PM systems. With MSB the number of required symbols reduces significantly, ranging from 5,000 to 12,000 symbols depending on the number of sub-bands and the corresponding equalizer length and step size. Although the MSB system requires a lower number of symbols to reach convergence, the overall convergence time should take into account the fact that the symbol period is also scaled by the number of sub-bands. The convergence time (in microseconds) for the MSB and SC systems is shown in Fig. 6(b), and reveals no evident relationship with the number of sub-bands. Both figures indicate a systematic BER penalty in the MSB transceiver compared with the SC option after convergence because of inter-sub-band interference.

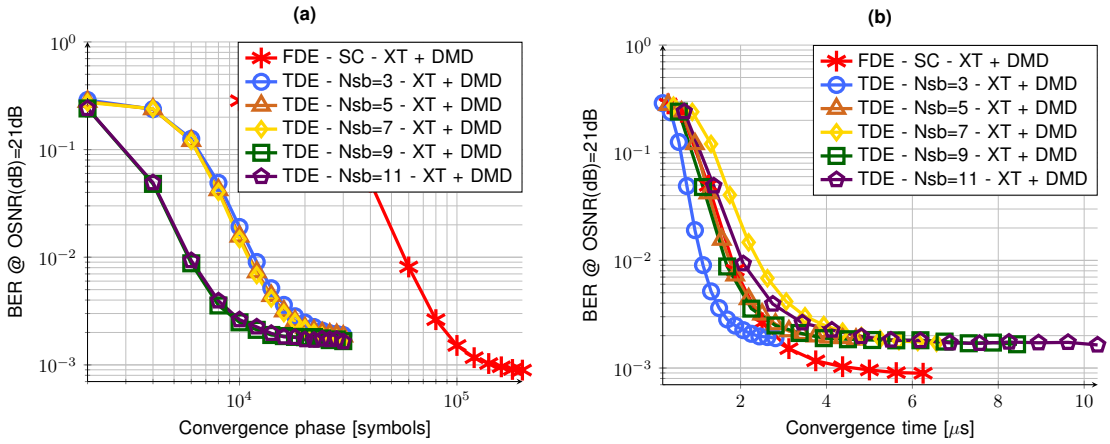

Fig. 6. Convergence period for OSNR = 21 dB of MSB and SC systems with -30 dB/km crosstalk and 20 ps/km DMD; (a) in number of symbols, and (b) in microseconds. Stars: SC system using FDE. Remaining symbols: MSB system for 3 (circles), 5 (triangles), 7 (diamonds), 9 (squares) and 11 (pentagons) sub-bands using TDE.

3.3. Dynamic channel performance

The dynamic channel model has the same parameters as the static one. However, after a sequence of 300,000 symbols, a polarization rotation is inserted using a simple 2×2 rotation matrix in each mode [35], given by:

$$R(\theta) = \begin{bmatrix} \cos(\theta) & -\sin(\theta) \\ \sin(\theta) & \cos(\theta) \end{bmatrix} \tag{2}$$

with θ=10^o. This value was selected so as to raise the bit error rate to values close to 10^{-2}, in a way to generate an error burst. System tracking performance is evaluated by BER estimated by means of the error vector magnitude (EVM) [36] computed over 512 symbols.

The BER for the SC and MSB systems subject to a polarization rotation with -30 dB/km crosstalk and 20 ps/km DMD are shown in Fig. 7, for varying step sizes (μ) and number of sub-bands. The link CD is fully compensated by static equalizers. The transient BER was estimated from the signal EVM averaged over all sub-bands. The purpose of this setup is to observe the response of the MSB system to a perturbation of the transmission channel, which in this case was implemented by a polarization rotation. As expected, excessively large step sizes lead to excess errors. For the SC system, approximately 0.6 μs are sufficient to ensure the transient recovery. During the transient, BER peaks higher than 10^{-2} are observed, potentially causing error bursts at reception. For the MSB system with 3 sub-bands the transient practically doubles, increasing the information loss period. The performance improves for 7 and 11 sub-bands, with a transient duration equivalent to the SC case.

3.4. Phase noise performance

This section investigates the impact of phase noise on the SC and MSB configurations. Phase noise follows a discrete Wiener process, in which the phase shift between adjacent symbols is a white Gaussian noise process with variance $\sigma_\theta^2 = 2\pi\Delta\nu T_s$, where T_s is the symbol period, and $\Delta\nu$ is the sum of transmitter and receiver laser linewidths. In MSB systems, the symbol period is directly proportional to the number of sub-bands, thus enhancing phase noise with an increasing number of sub-bands. To evaluate the impact of phase noise on the system performance we generate Wiener phase noise realizations that are replicated to all spatial modes, except of a constant random rotation. Phase recovery is carried out after the dynamic equalizer using the blind phase search (BPS) algorithm [37] with a 0.92 noise-rejection forgetting factor and 32 test

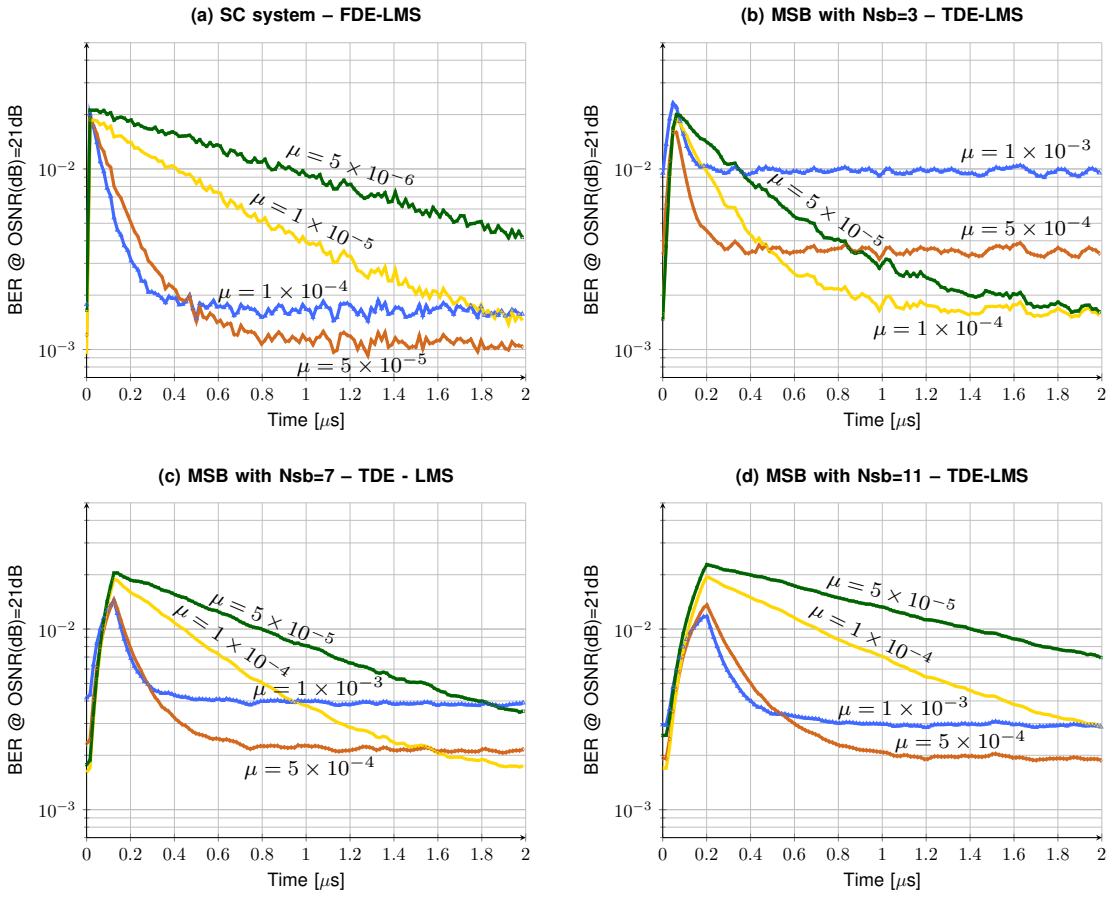

Fig. 7. (a) Convergence performance after perturbation of the SC system using FDE-LMS with different step sizes. (b)–(d) Convergence performance after perturbation of a MSB system with 3, 7 and 11 sub-bands using TDE-LMS with different step sizes. The simulated channel includes -30 dB/km crosstalk, 20 ps/km DMD. The CD is fully compensated by static equalizers. The resolution in time is 0.015 μs.

phases. Differential encoding and decoding is deployed to avoid cycle slips [38], [39]. We use a 200,000-symbols convergence phase for the SC-FDE system, where the first 20,000 symbols are processed by a supervised LMS algorithm, and the remaining 180,000 symbols resort to supervised radius directed equalization (RDE) [40] for calculating the error signal. For the MSB-TDE system, the 30,000-symbols-convergence phase consists of 10,000 symbols processed by a supervised LMS, and the remaining 20,000 symbols by supervised RDE. The equalizer step sizes have been optimized for each condition considering a 21-dB OSNR, and the filter lengths were selected according to Fig. 5.

Figure 8 shows the impact of phase noise on the SC and MSB systems, with DMD and fully compensated CD, for different linewidths (0, 25, 100 and 200 kHz). The system performance is evaluated in terms of $OSNR_{req}$ versus the number of sub-bands. Note that there is an intrinsic 1-dB penalty compared with the noise-loading case in Fig. 5(a) because of the BPS implementation, and the deployment of differential encoding and decoding. From the results in Fig. 8 note that phase noise impact on the SC system is negligible. The MSB solution without phase noise exhibits the expected 0.5-dB penalty with respect to the SC case, raising $OSNR_{req}$ from 20.5 dB to 21 dB. Using a 25-kHz laser, such as in [13], incurs an additional 0.2 dB penalty, with no noteworthy dependency on the number of sub-bands. With a 100-kHz laser linewidth the penalty raises with an

increasing number of sub-bands, ranging from 0.9 dB at 3 sub-bands to 1.3 dB at 11 sub-bands. For a 200-kHz linewidth the penalties are considerably higher. Joint-sub-band phase recovery can alleviate the impact of phase noise in MSB systems [41], [42], [43], but this solution may impair the parallel nature of this type of implementation. Finally, it should be noted that, although the phase noise penalties in systems with a high number of sub-bands can be non-negligible, they can be further suppressed with lower linewidth lasers, or higher symbol rates, which is a trend in high-bit-rate systems.

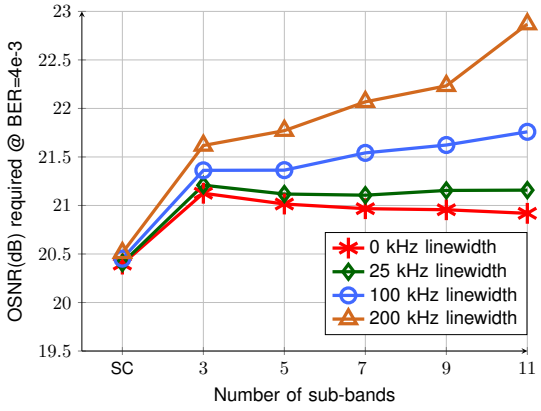

Fig. 8. Phase noise impact on the SC and MSB systems with crosstalk and DMD.

4. Computational Complexity

We evaluated the complexity of the SC-FDE system with that of the MSB-TDE architecture in terms of complex multiplications per bit. The computational complexity due to additions is neglected. We assumed that all K-point IFFTs/FFTs are implemented by the radix-2 algorithm, which requires nearly $K\log_2(K)/2$ complex multiplications [44].

4.1. Complexity of SC Transceiver

At the transmitter, the SC system has an RRC shaping filter with N_{RRC} coefficients per mode. The filter needs N_{RRC} complex multiplications to produce one output sample. Thus, the SC transmitter complexity is computed as:

$$C_{SC\_TX} = \frac{N_{\mathrm{RRC}}\mathrm{SPS}_{\mathrm{RRC}}}{\log_2 M} \tag{3}$$

where M is the modulation order and $\mathrm{SPS}_{\mathrm{RRC}}$ is the oversampling factor of the RRC filter.

For calculating the receiver complexity we assume FDE equalization using an extended version of the algorithm structure described in [29], applying the overlap-save method with 50% overlap. The update of adaptive filter coefficients is carried out by the LMS algorithm. At first, an input block with $2N_{\mathrm{FDE}}$ samples for each mode is divided into two blocks with N_{FDE} samples corresponding to odd and even samples that are processed separately. This structure requires $2N_m^2$ filters for MIMO processing (N_m^2 for the even samples and N_m^2 for the odd samples). Each of the $2N_m$ input blocks of N_{FDE} samples is subject to an FFT, yielding $N_m N_{\mathrm{FDE}}\log_2(N_{\mathrm{FDE}})$ complex multiplications. This is followed by the internal product by the filter coefficients, requiring $2N_m^2 N_{\mathrm{FDE}}$ complex multiplications. Subsequently, the outputs of the filters are added, producing N_m outputs. The N_m signals are converted back to time domain by N_m IFFTs, requiring $N_m N_{\mathrm{FDE}}\log_2(N_{\mathrm{FDE}})/2$ complex multiplications. For filter updating, the error calculation requires one FFT for each of the N_m outputs, yielding $N_m N_{\mathrm{FDE}}\log_2(N_{\mathrm{FDE}})/2$ complex multiplications. The gradient calculation implemented in [29] requires one IFFT and N_{FDE} complex multiplications for each of the $2N_m^2$ filters, requiring $(N_m^2 N_{\mathrm{FDE}}\log_2(N_{\mathrm{FDE}}) + 2N_m^2 N_{\mathrm{FDE}})$ complex multiplications. Finally, the filter

coefficient updating needs one FFT for each the $2N_m^2$ filters, resulting in $N_m^2 N_{\mathrm{FDE}} \log_2(N_{\mathrm{FDE}})$ complex multiplications. These operations produce $N_m N_{\mathrm{FDE}} \log_2(M)/2$ bits, considering the 50% overlap and a decimation in frequency domain by a factor of 2. Therefore, the receiver complexity, measured in complex multiplications per bit, can be calculated as:

$$C_{\mathrm{SC\_RX}} = C_{\mathrm{FDE}} = \frac{(4N_m + 4)\log_2 N_{\mathrm{FDE}} + 8N_m}{\log_2 M} \tag{4}$$

Finally, the complexity of the SC-FDE transceiver is given by:

$$C_{SC} = C_{\mathrm{SC\_TX}} + C_{\mathrm{SC\_RX}} = \frac{N_{\mathrm{RRC}} \mathrm{SPS}_{\mathrm{RRC}} + (4N_m + 4)\log_2 N_{\mathrm{FDE}} + 8N_m}{\log_2 M} \tag{5}$$

4.2. Complexity of MSB Transceiver

The MSB transmitter processes N_{sb} input symbols per mode with prototype filters of N_{pol} coefficients. The $(N_{sb}+1)$-point FFT at the input of the polyphase filter requires $(N_{sb}+1)\log_2(N_{sb}+1)/2$ complex multiplications. The output symbols are processed in the time domain by shaping filters requiring $(N_{sb}+1)N_{\mathrm{pol}}$ complex multiplications (see Fig. 2). Thus, the transmitter complexity can be calculated as:

$$C_{\mathrm{FB\_TX}} = \frac{(N_{sb}+1)[\log_2(N_{sb}+1) + 2N_{\mathrm{pol}}]}{2N_{sb}\log_2 M} \tag{6}$$

At the receiver [15], the polyphase filter processes blocks of $N_{sb}+1$ input samples. The twice-underdecimated architecture requires $2(N_{sb}+1)N_{\mathrm{pol}}$ complex multiplications to implement matched filters and additionally contains 2 IFFTs of $(N_{sb}+1)$ points, demanding $(N_{sb}+1)\log_2(N_{sb}+1)$ complex multiplications. At its output, the polyphase structure produces $2N_{sb}$ output samples, which generate N_{sb} symbols after MIMO processing and phase recovery. Thus, the filter bank complexity is given by:

$$C_{\mathrm{FB\_RX}} = \frac{(N_{sb}+1)[2N_{\mathrm{pol}} + \log_2(N_{sb}+1)]}{N_{sb}\log_2 M} \tag{7}$$

The TDE-LMS MIMO equalizer operates in time domain with N_{TDE} coefficients and two samples per symbol. The MIMO equalizer for each sub-band needs $N_m^2 N_{\mathrm{TDE}}$ complex multiplications for filtering, and $N_m^2 N_{\mathrm{TDE}}$ complex multiplications to update its coefficients. We assume that these operations are calculated only once within a symbol period [45]. Therefore, the TDE-LMS complexity is given by:

$$C_{\mathrm{TDE}} = \frac{2N_m N_{\mathrm{TDE}}}{\log_2 M} \tag{8}$$

Finally, the overall MSB transceiver complexity can be calculated as:

$$C_{\mathrm{MSB}} = C_{\mathrm{FB\_TX}} + C_{\mathrm{FB\_RX}} + C_{\mathrm{TDE}} = \frac{(N_{sb}+1)[3\log_2(N_{sb}+1) + 6N_{\mathrm{pol}}] + 4N_{sb}N_m N_{\mathrm{TDE}}}{2N_{sb}\log_2 M} \tag{9}$$

4.3. Complexity Comparison

We compare the complexity of the SC and MSB transceivers based on a case study whose parameters are obtained from the simulation results presented in Section 3. The results, shown in Table I, assume an optical channel with CD, crosstalk and DMD. The input parameters for Eqs. 5 and 9 are N_m = 12 modes, M = 16 (16-QAM), Nyquist-pulse shaping with N_{RRC} = 65 taps and $SPS_{\mathrm{RRC}} = 2$ samples per symbol for SC, and polyphase filters with N_{pol}= 128 taps for MSB. The length of adaptive equalizers, shown Table I, were obtained from the performance curves presented in Figs. 5(b) and 5(d).

Clearly, an increasing number of sub-bands reduces the complexity of the MSB transceiver: 3 sub-bands requires 549 complex multiplications per symbol, whereas for 11 sub-bands this number is reduced to 286. However, the best case for MSB (N_{sb} =11) still requires 1.8 times the complexity of a SC-FDE architecture. Since the link length is relatively small, the gains provided by the MSB architecture for CD compensation were not significant.

TABLE I
COMPLEXITY COMPARISON BETWEEN SC AND MSB TRANSCEIVERS.

DESCRIPTION	SC	MSB				
		$N_{sb} = 3$	$N_{sb} = 5$	$N_{sb} = 7$	$N_{sb} = 9$	$N_{sb} = 11$
Equalizer length (taps)	280	70	50	40	30	30
Complexity (multiplications/bit)	162	549	416	351	288	286
Relative complexity	1	3.4	2.6	2.2	1.8	1.8

5. Conclusion

We compare the performance of MSB transmission implemented by filter banks and TDE, to that of SC architectures using FDE, for systems with mode multiplexing. The MSB architecture allows parallelizing MIMO equalization and the subsequent DSP steps, enabling practical implementations. The evaluated scenarios include the effects of CD, crosstalk, DMD, and additive noise. The simulation results indicate that, for a configuration with noise loading only, the MSB implementation has a penalty of approximately 0.5 dB compared to the SC system due to interference between the sub-bands. In the simulation of fiber effects, the MSB system allows to work with shorter equalizers, as expected. The duration of the convergence phase of MSB systems was shown to be equivalent to that of the SC system. Similarly, the responsiveness of the MSB system to perturbations was dependent on the number of sub-bands, but still with no significant difference in relation to SC systems. We also evaluated the impact of phase noise on the SC and MSB systems. As expected, the results indicate an increasing penalty with a growing number of sub-bands for large linewidth lasers. This effect can be alleviated by joint-sub-carrier phase recovery, lower linewidth lasers, or an increase in the system symbol rate. In terms of complexity, the MSB architecture exhibited a higher complexity, with an increasing performance for a high number of sub-bands. Finally, compared with the SC system, the MSB architecture offers high parallelism (e.g. 11 sub-bands) at cost of a penalty of 0.7-to-1.3 dB for a laser linewidth of 25-to-100 kHz and a moderate increase in complexity (e.g. 1.8 times at 11 sub-bands).

Acknowledgements

At UNICAMP, this work was supported by CAPES, and FAPESP grants 2015/24341-7 and 2015/24517-8. At Aston University, this work has been partially supported by the EU (619732-INSPACE and 654809-HSPACE), and by EPSRC (EP/L000091/1-PEACE).

References

[1] L. F. dos Santos, F. M. Ferreira, and D. A. A. Mello, "Sub-band-based transmission for mode-multiplexed optical systems," in *2017 19th International Conference on Transparent Optical Networks (ICTON)*, Jul. 2017, pp. 1–4.

[2] R. Ryf, S. Randel, A. H. Gnauck, C. Bolle, R. J. Essiambre, P. J. Winzer, D. W. Peckham, A. McCurdy, and R. Lingle, "Space-division multiplexing over 10 km of three-mode fiber using coherent 6 x 6 MIMO processing," in *Proc. Optical Fiber Communication Conference and Exposition and the National Fiber Optic Engineers Conference (OFC/NFOEC)*, Mar. 2011, p. PDPB10.

[3] R. Ryf *et al.*, "12 x 12 MIMO transmission over 130-km few-mode fiber," in *Frontiers in Optics 2012 Laser Science XXVIII*. The Optical Society (OSA), 2012, p. FW6C.4.

[4] N. K. Fontaine *et al.*, "30 x 30 MIMO transmission over 15 spatial modes," in *Proc. Optical Fiber Communications Conference (OFC)*, Mar. 2015, p. Th5C.1.

[5] M. B. Shemirani, W. Mao, R. A. Panicker, and J. M. Kahn, "Principal modes in graded-index multimode fiber in presence of spatial- and polarization-mode coupling," *Journal of Lightwave Technology*, vol. 27, no. 10, pp. 1248–1261, May 2009.

[6] K.-P. Ho and J. M. Khan, "Mode coupling and its impact on spatially multiplexed systems," *Optical Fiber Telecommunications VI, B, I. P. Kaminow, T. Li, and A. E. Willner, Eds.*, vol. ch11, pp. 491–568, 2013.

[7] S. O. Arik, D. Askarov, and J. M. Kahn, "Effect of mode coupling on signal processing complexity in mode-division multiplexing," *Journal of Lightwave Technology*, vol. 31, no. 3, pp. 423–431, Feb. 2013.

[8] S. Randel, P. J. Winzer, M. Montoliu, and R. Ryf, "Complexity analysis of adaptive frequency-domain equalization for MIMO-SDM transmission," in *Proc. 39th European Conference and Exhibition on Optical Communication (ECOC)*, Sept. 2013, pp. 1–3.

[9] N. Bai, E. Ip, M. Li, T. Wang, and G. Li, "Experimental demonstration of adaptive frequency-domain equalization for mode-division multiplexed transmission," in *Proc. Optical Fiber Communication Conference and Exposition and the National Fiber Optic Engineers Conference (OFC/NFOEC)*, Mar. 2013, p. OM2C.5.

[10] M. Nazarathy and A. Tolmachev, "Digital sub-banding for coherent single-mode and spatial division multiplexed fiber systems," in *Proc. OptoElectronics and Communication Conference and Australian Conference on Optical Fibre Technology (OECC/ACOFT)*, Jul. 2014, pp. 374–376.

[11] K. P. Ho, "Subband equaliser for chromatic dispersion of optical fibre," *Electronics Letters*, vol. 45, no. 24, pp. 1224–1226, Nov. 2009.

[12] T. Mizuno *et al.*, "12-core x 3-mode dense space division multiplexed transmission over 40 km employing multi-carrier signals with parallel mimo equalization," in *Proc. Optical Fiber Communication Conference (OFC)*, Mar. 2014, p. Th5B.2.

[13] K. Shibahara *et al.*, "Dense SDM (12-core $\times$ 3-mode) transmission over 527 km with 33.2-ns mode-dispersion employing low-complexity parallel mimo frequency-domain equalization," *Journal of Lightwave Technology*, vol. 34, no. 1, pp. 196–204, Jan. 2016.

[14] B. Farhang-Boroujeny, "OFDM versus filter bank multicarrier," *IEEE Signal Processing Magazine*, vol. 28, no. 3, pp. 92–112, May 2011.

[15] M. Nazarathy and A. Tolmachev, "Subbanded DSP architectures based on underdecimated filter banks for coherent OFDM receivers: overview and recent advances," *IEEE Signal Processing Magazine*, vol. 31, no. 2, pp. 70–81, Mar. 2014.

[16] I. Slim, A. Mezghani, L. G. Baltar, J. Qi, F. N. Hauske, and J. A. Nossek, "Delayed single-tap frequency-domain chromatic-dispersion compensation," *IEEE Photonics Technology Letters*, vol. 25, no. 2, pp. 167–170, Jan. 2013.

[17] M. Malekiha, I. Tselniker, and D. V. Plant, "Chromatic dispersion mitigation in long-haul fiber-optic communication networks by sub-band partitioning," *Optics Express*, vol. 23, no. 25, pp. 32 654–32 663, 2015.

[18] M. Malekiha and D. V. Plant, "Complexity reduction of dispersion mitigation based on sub-band partitioning," in *Proc. 2016 Photonics North (PN)*, Mar. 2016, pp. 1–2.

[19] Y. Tang, W. Shieh, and B. S. Krongold, "DFT-spread OFDM for fiber nonlinearity mitigation," *IEEE Photonics Technology Letters*, vol. 22, no. 16, pp. 1250–1252, Aug. 2010.

[20] M. Qiu, Q. Zhuge, M. Chagnon, Y. Gao, X. Xu, M. Morsy-Osman, and D. V. Plant, "Digital subcarrier multiplexing for fiber nonlinearity mitigation in coherent optical communication systems," *Optics Express*, vol. 22, no. 15, pp. 18 770–18 777, Jul. 2014.

[21] M. Qiu, Q. Zhuge, X. Xu, M. Chagnon, M. Morsy-Osman, and D. V. Plant, "Subcarrier multiplexing using DACs for fiber nonlinearity mitigation in coherent optical communication systems," in *Proc. Optical Fiber Communication Conference (OFC)*, Mar. 2014, p. Tu3J.2.

[22] D. Krause, A. Awadalla, A. S. Karar, H. Sun, and K. T. Wu, "Design considerations for a digital subcarrier coherent optical modem," in *Proc. Optical Fiber Communications Conference (OFC)*, Mar. 2017, p. Th1D.1.

[23] M. Seimetz, "Multi-format transmitters for coherent optical M-psk and M-qam transmission," in *Proc. 7th International Conference Transparent Optical Networks (ICTON)*, vol. 2, Jul. 2005, pp. 225–229 Vol. 2.

[24] F. J. Harris, *Multirate Signal Processing for Communication Systems*. Prentice Hall, 2004.

[25] A. V. Oppenheim and R. W. Schafer with J. R. Buck, *Discrete-Time Signal Processing*, 2nd ed. Prentice Hall, 1999.

[26] A. R. Shah, R. C. J. Hsu, A. Tarighat, A. H. Sayed, and B. Jalali, "Coherent optical MIMO (COMIMO)," *Journal of Lightwave Technology*, vol. 23, no. 8, pp. 2410–2419, Aug. 2005.

[27] S. J. Savory, "Digital coherent optical receivers: Algorithms and subsystems," *IEEE Journal of Selected Topics in Quantum Electronics*, vol. 16, no. 5, pp. 1164–1179, Sept. 2010.

[28] ——, "Digital filters for coherent optical receivers," *Optics Express*, vol. 16, pp. 804–817, 2008.

[29] M. S. Faruk and K. Kikuchi, "Adaptive frequency-domain equalization in digital coherent optical receivers," *Opt. Express*, vol. 19, no. 13, pp. 12 789–12 798, June 2011.

[30] F. Ferreira, P. Monteiro, and H. Silva, "Semi-analytical model for linear modal coupling in few-mode fiber transmission," in *Proc. 14th International Conference on Transparent Optical Networks (ICTON)*, Jul. 2012, p. Th.A1.5.

[31] F. M. Ferreira, C. S. Costa, S. Sygletos, and A. D. Ellis, "Semi-analytical modelling of linear mode coupling in few-mode fibers," *Journal of Lightwave Technology*, vol. 35, no. 18, pp. 4011–4022, Sept. 2017.

[32] F. M. Ferreira, N. M. Suibhne, S. Sygletos, and A. D. Ellis, "Few-mode fibre group-delays with intermediate coupling," in *Proc. European Conference on Optical Communication (ECOC)*, Sept. 2015, pp. 1–3.

[33] F. M. Ferreira, D. Fonseca, and H. J. A. da Silva, "Design of few-mode fibers with m-modes and low differential mode delay," *Journal of Lightwave Technology*, vol. 32, no. 3, pp. 353–360, Feb. 2014.

[34] B. Widrow, J. McCool, and M. Ball, "The complex LMS algorithm," *Proceedings of the IEEE*, vol. 63, no. 4, pp. 719–720, Apr. 1975.

[35] B. Szafraniec, T. S. Marshall, and B. Nebendahl, "Performance monitoring and measurement techniques for coherent optical systems," *Journal of Lightwave Technology*, vol. 31, no. 4, pp. 648–663, Feb. 2013.

[36] "Technical report 61282-10: Fibre optic communication system design guides part 10: characterization of the quality of optical vector-modulated signals with error vector magnitude," International Electrotechnical Commission (IEC), Jan. 2013.

[37] A. A. Payyazh, A. L. N. de Souza, and D. A. A. Mello, "Recursive blind phase search architecture for phase recovery at high error rates," in *2018 International Optics and Photonics Conference (SBFoton)*, Oct. 2018, pp. 1–5.

[38] W. Weber, "Differential encoding for multiple amplitude and phase shift keying systems," *IEEE Transactions on Communications*, vol. 26, no. 3, pp. 385–391, Mar. 1978.

[39] I. Fatadin, D. Ives, and S. J. Savory, "Compensation of frequency offset for differentially encoded 16- and 64-qam in the presence of laser phase noise," *IEEE Photonics Technology Letters*, vol. 22, no. 3, pp. 176–178, Feb. 2010.
[40] M. J. Ready and R. P. Gooch, "Blind equalization based on radius directed adaptation," in *International Conference on Acoustics, Speech, and Signal Processing*, Apr. 1990, pp. 1699–1702 vol.3.
[41] D. V. Souto, B. Olsson, C. Larsson, and D. A. A. Mello, "Joint-polarization and joint-subchannel carrier phase estimation for 16-qam optical systems," *Journal of Lightwave Technology*, vol. 30, no. 20, pp. 3185–3191, Oct. 2012.
[42] M. Qiu, Q. Zhuge, M. Chagnon, F. Zhang, and D. V. Plant, "Laser phase noise effects and joint carrier phase recovery in coherent optical transmissions with digital subcarrier multiplexing," *IEEE Photonics Journal*, vol. 9, no. 1, pp. 1–13, Feb. 2017.
[43] M. P. Yankov, L. Barletta, and D. Zibar, "Phase noise compensation for nonlinearity-tolerant digital subcarrier systems with high-order qam," *IEEE Photonics Journal*, vol. 9, no. 5, pp. 1–12, Oct. 2017.
[44] N. Benvenuto and G. Cherubini, *Algorithms for Communications Systems and Their Applications*. John Wiley & Sons, 2002.
[45] B. Inan, B. Spinnler, F. Ferreira, D. van den Borne, A. Lobato, S. Adhikari, V. A. J. M. Sleiffer, M. Kuschnerov, N. Hanik, and S. L. Jansen, "DSP complexity of mode-division multiplexed receivers," *Opt. Express*, vol. 20, no. 10, pp. 10 859–10 869, May 2012.